

MAFNet: Multi-frequency Adaptive Fusion Network for Real-time Stereo Matching

Ao Xu², Rujin Zhao^{3,6}, Xiong Xu^{1,2,4,5}, Boceng Huang¹, Yujia Jia²
Hongfeng Long³, Fuxuan Chen¹, Zilong Cao¹, Fangyuan Chen

¹College of Surveying and Geo-Informatics, Tongji University, Shanghai, China

²Shanghai Research Institute for Intelligent Autonomous Systems, Tongji University, Shanghai, China

³Institute of Optics and Electronics, Chinese Academy of Sciences, Chengdu 610209, China

⁴Shanghai Integrated Innovation Center for Manned Lunar Exploration, Shanghai, China

⁵Shanghai Key Laboratory for Planetary Mapping and Remote Sensing for Deep Space Exploration, Shanghai, China

⁶University of Chinese Academy of Sciences, Beijing 100049, China

Abstract—Existing stereo matching networks typically rely on either cost-volume construction based on 3D convolutions or deformation methods based on iterative optimization. The former incurs significant computational overhead during cost aggregation, whereas the latter often lacks the ability to model non-local contextual information. These methods exhibit poor compatibility on resource-constrained mobile devices, limiting their deployment in real-time applications. To address this, we propose a Multi-frequency Adaptive Fusion Network (MAFNet), which can produce high-quality disparity maps using only efficient 2D convolutions. Specifically, we design an adaptive frequency-domain filtering attention module that decomposes the full cost volume into high-frequency and low-frequency volumes. Subsequently, we introduce a Linformer-based low-rank attention to adaptively aggregate high- and low-frequency information, yielding more robust disparity estimation. Extensive experiments demonstrate that the proposed MAFNet significantly outperforms existing real-time methods on public datasets such as Scene Flow and KITTI 2015, showing a favorable balance between accuracy and real-time performance. Code: <https://anonymous.4open.science/r/MAFNet-B05E>.

Index Terms—Stereo matching, 3D vision, Real-Time depth estimation

I. INTRODUCTION

With the advent of autonomous driving, drone inspection, smart manufacturing, augmented reality, and medical robotics, acquiring accurate 3D structural information has become essential for intelligent perception systems [1]–[5]. Stereo matching, which estimates scene depth by establishing pixel correspondences between rectified image pairs under geometric constraints, is a key component of 3D vision [6]. Leveraging deep learning, end-to-end stereo networks [7]–[10] have achieved state-of-the-art results on benchmarks such as Scene Flow [11] and KITTI [12], driving the adoption of 3D vision across research and industry.

Recent studies have extensively explored cost-volume construction and representation to improve stereo matching [13], [14]. Representative methods include GwcNet [15], which computes group-wise correlations to form more discriminative

volumes; ACVNet [16], which introduces attention mechanisms to convert correlation volumes into attention weights for finer filtering; and PCWNet [17], which combines pyramidal structures with deformable volumes for enhanced multi-scale modeling. While these approaches significantly boost accuracy, their reliance on high-resolution volumes and large-scale 3D convolutions incurs heavy computational and memory costs, hindering real-time deployment on resource-constrained mobile or embedded platforms.

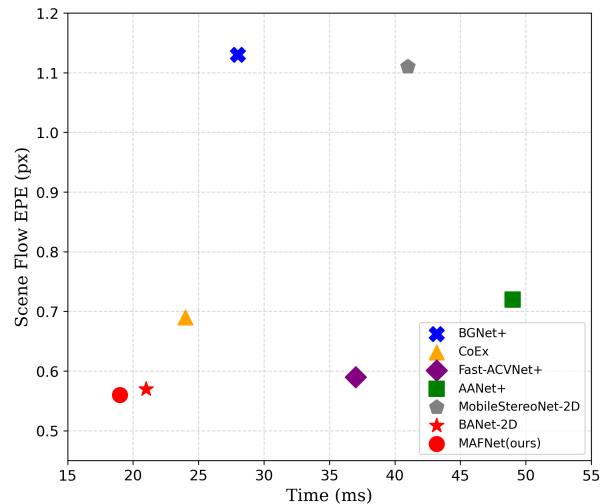


Fig. 1. Comparison with state-of-the-art real-time methods on the Scene Flow (4090GPU).

To improve efficiency, subsequent studies have introduced lightweight strategies such as constructing lower-resolution cost volumes, adopting sparse disparity searches, and employing lightweight aggregation networks like StereoNet [18], DeepPruner [19], and Fast-ACVNet [20]. While these methods achieve faster inference on high-end GPUs, they still depend on extensive 3D convolutions or complex deformable operations, limiting deployment on mobile platforms, as shown in Fig. 1. Another line of work replaces 3D with 2D convolu-

tions for cost aggregation, e.g., AANet [21] uses deformable convolutions for adaptive aggregation, and MobileStereoNet-2D [22] integrates lightweight MobileNet modules. Although these approaches improve efficiency, they remain prone to errors in blurred textures, textureless regions, and fine edges, leading to noticeable detail loss.

To overcome these limitations, MAFNet introduces an adaptive frequency-domain attention to explicitly separate high-frequency details from low-frequency regions and a Linformer-based fusion module for lightweight, dynamic aggregation. This design retains the efficiency of 2D convolutions while strengthening the modeling of complex textures and edges, thus achieving a better trade-off between real-time performance and accuracy and making the network well suited for edge or mobile deployment. Our contributions are as follows:

- We propose MAFNet, a lightweight stereo matching framework that achieves accurate disparity estimation using only 2D convolutions, enabling efficient deployment on mobile and edge devices.
- An Adaptive Frequency-Domain Filtering Attention (AFFA) module is introduced to separate high-frequency details from low-frequency smooth regions, reducing errors in textureless areas and near thin edges.
- An Adaptive Aggregation of High- and Low-Frequency (AAHF) module is designed based on a Linformer architecture to enable global feature interaction with low computational cost, achieving a better balance between runtime efficiency and prediction accuracy compared with existing mobile-oriented methods.

II. METHOD

A. Model Architecture

Feature Extraction. As shown in Fig. 2, our network takes a pair of rectified images as input and first extracts multi-scale high-dimensional features using a weight-sharing MobileNetv2 backbone. Specifically, feature maps are obtained at four scales: 1/4, 1/8, 1/16, and 1/32 of the original resolution. Starting from the 1/32-resolution features, we progressively upsample to 1/4 resolution via transposed convolutions with a 4x4 kernel and stride 2, producing multi-scale features f_l, f_r for the left and right images, with three key scales (1/4, 1/8, 1/16) retained. The multi-scale features of the left image are fed into an adaptive frequency-domain filtering attention module to generate frequency-aware spatial weights, while the 1/4-resolution features of both images are used to construct the cost volume.

Cost Volume Construction. Given the quarter-resolution feature maps of the left and right images, $f_{l,4}, f_{r,4} \in \mathbb{R}^{B \times N_c \times H/4 \times W/4}$, we construct the group-wise correlation volume by first evenly dividing the feature channels into N_g groups, each containing N_c/N_g channels, which is defined as:

$$C(x, y, d, g) = \frac{1}{N_c/N_g} \left\langle f_{l,4}^{(g)}(x, y), f_{r,4}^{(g)}(x - d, y) \right\rangle, \quad (1)$$

where (x, y) denotes the spatial location, $\langle \cdot, \cdot \rangle$ denotes the inner product, $d \in \mathcal{D} = \{0, 1, 2, \dots, D/4 - 1\}$ is the disparity index, $g \in \{1, 2, \dots, N_g\}$ denotes the group index.

Disparity Prediction. The proposed AFFA is used to construct the high- and low-frequency cost volumes. The aggregated cost volume is then obtained through the proposed AAHF module, followed by a softmax operation for disparity regression to produce the final disparity map d_0 . The architectural details of the AFFA and AAHF modules are presented in Sec. 2.2 and 2.3, respectively:

$$D_0 = \sum_{d=0}^{D/4-1} d \times \text{Softmax}(C_{\text{AAHF}}(d)), \quad (2)$$

where D denotes the predefined maximum disparity, and d indexes the disparity candidates within the range $[0, D/4 - 1]$. The predicted disparity map D_0 is obtained at a resolution of $H/4 \times W/4$. To recover a full-resolution result, superpixel-based weights are applied around each pixel in the left image to aggregate local neighboring values in D_0 , yielding the final disparity map $D_1 \in \mathbb{R}^{H \times W}$.

Loss Function. The entire network is trained in a supervised end-to-end manner, and the final loss function is defined as:

$$L = \lambda_0 L_{1\text{-smooth}}(D_0 - D_{gt}^{1/4}) + \lambda_1 L_{1\text{-smooth}}(D_1 - D_{gt}) \quad (3)$$

where D_{gt} denotes the ground-truth disparity map and $L_{1\text{-smooth}}$ is the smooth L1 loss. $D_{gt}^{1/4}$ represents the ground-truth disparity downsampled to 1/4 resolution. D_0 and D_1 denote the predicted disparities at 1/4 and full resolution, respectively.

B. Adaptive Frequency-Domain Filtering Attention

High-frequency image components mainly encode fine details and edges, while low-frequency components capture global structures and textureless regions. To leverage these complementary features, we propose an adaptive frequency-domain filtering attention module. The module first decomposes feature maps in the frequency domain to obtain high- and low-frequency subbands. A learnable spatial gating mechanism is then applied to dynamically generate pixel-wise fusion weights for the two subbands. The resulting attention maps adaptively distinguish frequency characteristics across different regions, effectively enhancing edge fidelity and improving matching stability in textureless areas.

As illustrated in Fig. 3, given a feature map $X \in \mathbb{R}^{B \times C \times H \times W}$, we first compute its 2D Real Fast Fourier Transform (RFFT) to obtain the frequency-domain representation:

$$F(X) = \text{RFFT}(X), F(X) \in \mathbb{C}^{B \times C \times H \times W} \quad (4)$$

In the frequency plane, the low-frequency components are concentrated near the center while the high-frequency components are distributed toward the edges. We introduce learnable thresholds τ_l and τ_h to adaptively separate the bands and construct soft masks as:

$$M_{\text{low}}(u, v) = \sigma\left(\frac{\tau_l - r(u, v)}{\gamma}\right) \quad (5)$$

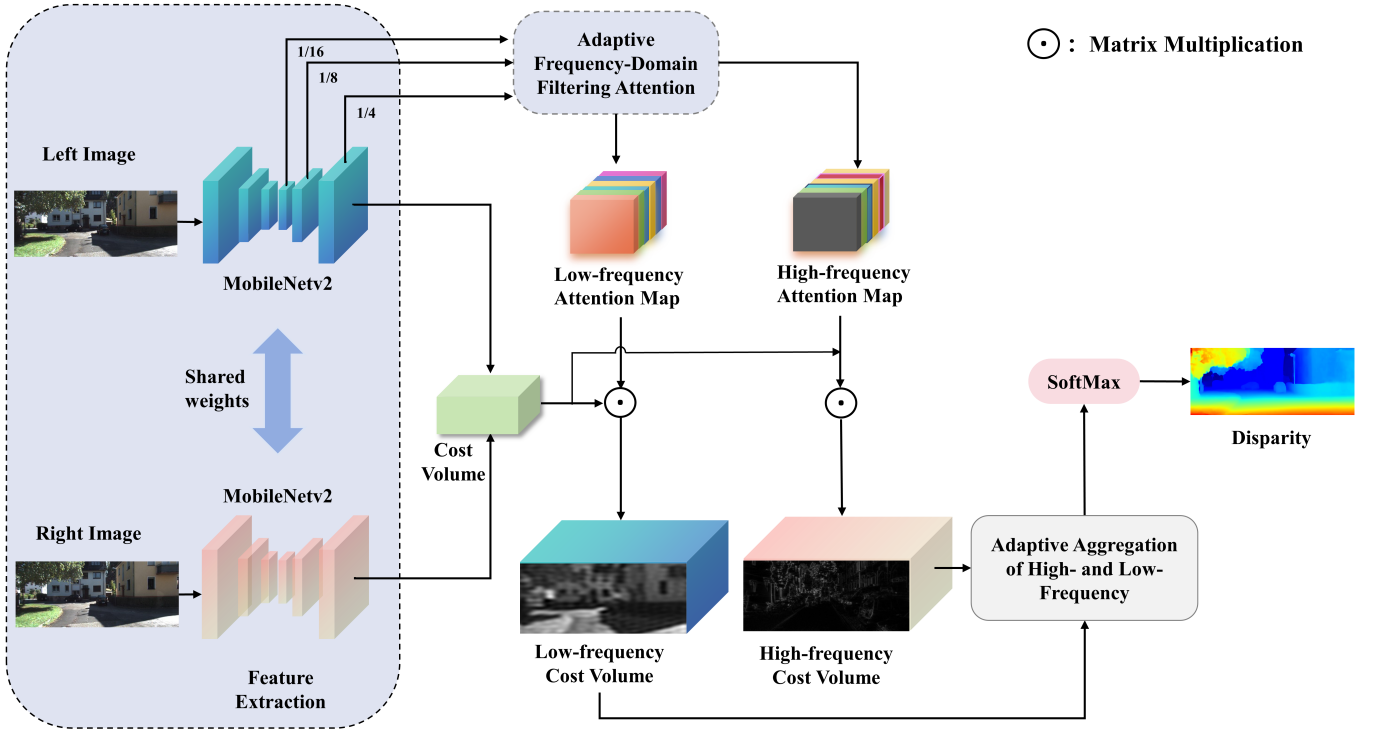


Fig. 2. Overview of the proposed network. Given a rectified stereo image pair, multi-scale features are extracted using a weight-sharing MobileNet2 backbone. An adaptive frequency-domain attention separates features into high- and low-frequency components, which are used to construct corresponding cost volumes. These cost volumes are aggregated by a high–low frequency adaptive fusion module, followed by disparity regression to generate the final disparity map.

TABLE I
RESULTS OF ABLATION EXPERIMENT ON THE SCENE FLOW DATASET.

Model	Adaptive Frequency-Domain Filtering Attention	Adaptive Aggregation of High- and Low-Frequency	EPE (px)	Bad 3.0 (%)	Param(M)
Baseline	×	×	0.64	2.87	3.69
AFFA	✓	×	0.58	2.53	3.81
AFFA+AAHF (MAFNet)	✓	✓	0.56	2.41	3.82

TABLE II
RESULTS OF ABLATION EXPERIMENT ON KITTI 2012 AND KITTI 2015 DATASETS.

Method	KITTI 2012			KITTI 2015	
	3-noc	3-all	D1-bg	D1-fg	D1-all
w/o AFFA	1.73	2.18	1.81	3.75	2.13
MAFNet	1.36	1.76	1.57	3.02 (19%↑)	1.81

$$M_{high}(u, v) = \sigma\left(\frac{r(u, v) - \tau_h}{\gamma}\right) \quad (6)$$

where $r(u, v)$ denotes the normalized radius from a frequency-domain point to the center, σ is the sigmoid function, and γ is the temperature parameter used to control the smoothness of the soft threshold. Thus, the high- and low-frequency decomposition is obtained:

$$X_{low} = IRFFT(F(X) \odot M_{low}) \quad (7)$$

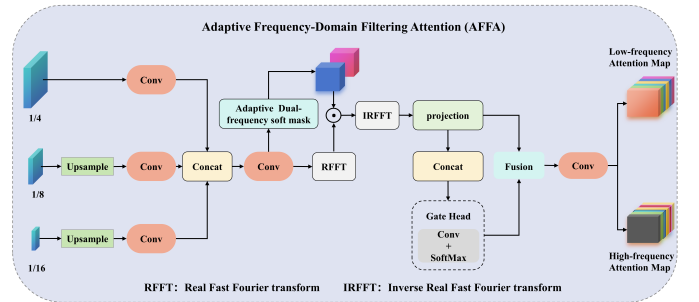


Fig. 3. AFFA Structure Diagram.

$$X_{high} = IRFFT(F(X) \odot M_{high}) \quad (8)$$

where IRFFT denotes the inverse real fast Fourier transform. To avoid the constraints introduced by fixed frequency band division, we propose a spatially adaptive gating mechanism.

Specifically, the high- and low-frequency features are first concatenated:

$$Z = \text{Concat}[X_{low}, X_{high}] \in \mathbb{R}^{B \times 2C \times H \times W} \quad (9)$$

Then, pixel-level weights are obtained via a 1×1 convolution:

$$G = \text{Softmax}(\text{Conv}_{1 \times 1}(Z)) \in \mathbb{R}^{B \times 2 \times H \times W} \quad (10)$$

$$G_{low} = G[:, 0, :, :], \quad G_{high} = G[:, 1, :, :] \quad (11)$$

The fused feature is given by:

$$X_f = G_{low} \odot X_{low} + G_{high} \odot X_{high} \quad (12)$$

Finally, convolutional layers followed by a sigmoid function are applied to generate the high- and low-frequency attention maps:

$$A_{high} = \sigma(\text{Conv}(X_f)) \quad (13)$$

$$A_{low} = 1 - A_{high} \quad (14)$$

C. Adaptive Aggregation of High- and Low-Frequency

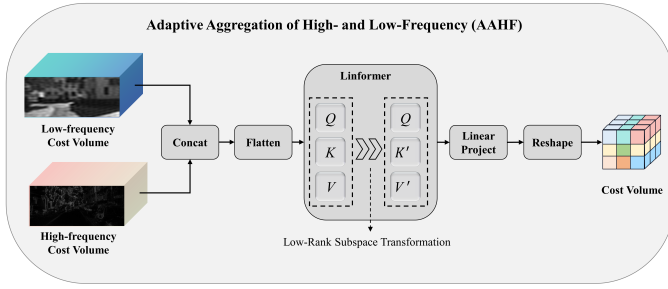


Fig. 4. AAHF Structure Diagram.

The high-frequency feature and low-frequency feature respectively capture detailed edges and smooth regions, and they are complementary in stereo matching. Simply using element-wise addition or multiplication for fusion often fails to adaptively adjust their contributions across different regions, resulting in insufficient feature aggregation. To address this, we introduce a Linformer-based adaptive fusion module, which employs low-rank attention mapping to achieve efficient and dynamic feature fusion.

Given the constructed raw cost volume C , it is decomposed into a high-frequency cost volume CV_{high} and a low-frequency cost volume CV_{low} :

$$\begin{aligned} CV_{high} &= A_{high} \odot C, \\ CV_{low} &= A_{low} \odot C \end{aligned} \quad (15)$$

As shown in Fig. 4, given the input high-frequency cost volume $CV_{high} \in \mathbb{R}^{B \times D \times H \times W}$ and low-frequency cost volume $CV_{low} \in \mathbb{R}^{B \times D \times H \times W}$, we first concatenate them to obtain:

$$CV_{all} = \text{Concat}(CV_{high}, CV_{low}) \in \mathbb{R}^{B \times 2D \times H \times W} \quad (16)$$

It is then flattened into a sequential representation:

$$X = \text{Reshape}(CV_{all}) \in \mathbb{R}^{B \times N \times 2D}, \quad N = H \times W \quad (17)$$

The standard self-attention is defined as:

$$\text{Att}(Q, K, V) = \text{SoftMax}\left(\frac{QK^T}{\sqrt{d}}\right)V \quad (18)$$

where $Q, K, V \in \mathbb{R}^{N \times d}$, with a computational complexity of $O(N^2)$. In Linformer, the key K and value V are projected into a low-rank subspace:

$$K' = EK, \quad V' = FV, \quad (E, F) \in \mathbb{R}^{k \times N}, \quad k \ll N \quad (19)$$

The attention computation is given by:

$$\text{LinAtt}(Q, K, V) = \text{Softmax}\left(\frac{QK'^T}{\sqrt{d}}\right)V' \quad (20)$$

The complexity is reduced to $O(N \cdot k)$. Through the low-rank approximation, the model can significantly reduce computational cost while maintaining representational capacity. Finally, we use a linear projection to map the output back to $\mathbb{R}^{B \times N \times D}$ and reshape it into the fused volume C_{AAHF} :

$$C_{AAHF} = \text{Reshape}(\text{LinAtt}(X)) \in \mathbb{R}^{B \times D \times H \times W} \quad (21)$$

III. EXPERIMENTS

A. Implementation Details and Datasets

The proposed MAFNet model was implemented using PyTorch, and experiments were carried out on the Scene Flow [11], KITTI 2012 [23], and KITTI 2015 [12] datasets. All experiments were conducted on an NVIDIA RTX 4090 GPU. We employed the AdamW [28] optimizer combined with a one-cycle learning rate scheduler with warm-up, setting the maximum learning rate to $8e-4$. The weights in the loss function were configured as $\lambda_0 = 0.3$ and $\lambda_1 = 1.0$. During training, we initially pre-trained on the Scene Flow dataset for 200k steps with a batch size of 16 to adequately learn the distribution of large-scale synthetic data. The resulting model was then fine-tuned for 50k steps on the mixed KITTI 2012 and KITTI 2015 training sets to improve performance in real-world environments. During training, each input image was randomly cropped to a resolution of 256×512 .

B. Ablation Study

Comprehensive ablation studies were carried out on Scene Flow [11] and KITTI [12], [23] to verify the effectiveness of the proposed approach, with the ablation results for Scene Flow presented in Table I and those for KITTI 2012 [23] and 2015 [12] presented in Table II. The baseline adopts a single-branch aggregation architecture. Without AFFA, the input to AAHF is a standard cost volume.

Table I presents the ablation study results evaluated on the Scene Flow dataset. The AFFA module decouples high-frequency details and low-frequency smooth regions, leading to a decrease in EPE from 0.64 to 0.58 and Bad 3.0 error from 2.87% to 2.53% while introducing only a marginal number of additional parameters. By further fusing multi-frequency information, the AAHF module lowers the EPE to 0.56 and the Bad 3.0 error to 2.41%, incurring an almost negligible increase in model parameters.

TABLE III
QUANTITATIVE COMPARISON ON THE KITTI 2012 AND KITTI 2015 BENCHMARKS.

Method	KITTI 2012 [23]						KITTI 2015 [12]			Time (ms)
	3-noc	3-all	4-noc	4-all	Avg-Noc	Avg-All	D1-bg	D1-fg	D1-all	
CoEx [24]	1.55	1.93	1.15	1.42	0.5	0.5	1.79	3.82	2.13	24
AANet+ [21]	1.55	2.04	1.20	1.58	0.4	0.5	1.65	3.96	2.03	49
DeepPruner-Fast [19]	–	–	–	–	–	–	2.32	3.91	2.59	43
Fast-ACVNet [16]	1.68	2.13	1.23	1.56	0.5	0.6	1.82	3.93	2.17	31
Fast-ACVNet+ [16]	1.45	1.85	1.06	1.36	0.5	0.5	1.70	3.53	2.01	37
HITNet [25]	1.41	1.89	1.14	1.53	0.4	0.5	1.74	3.20	1.98	12
MobileStereoNet-2D [22]	–	–	–	–	–	–	2.49	4.53	2.83	41
BGNet+ [26]	1.62	2.03	1.16	1.48	0.5	0.6	1.81	4.09	2.19	28
BANet-2D [27]	1.38	1.79	1.01	1.32	0.5	0.5	1.59	3.03	1.83	21
MAFNet (Ours)	1.36	1.76	0.98	1.31	0.5	0.5	1.57	3.02	1.81	19

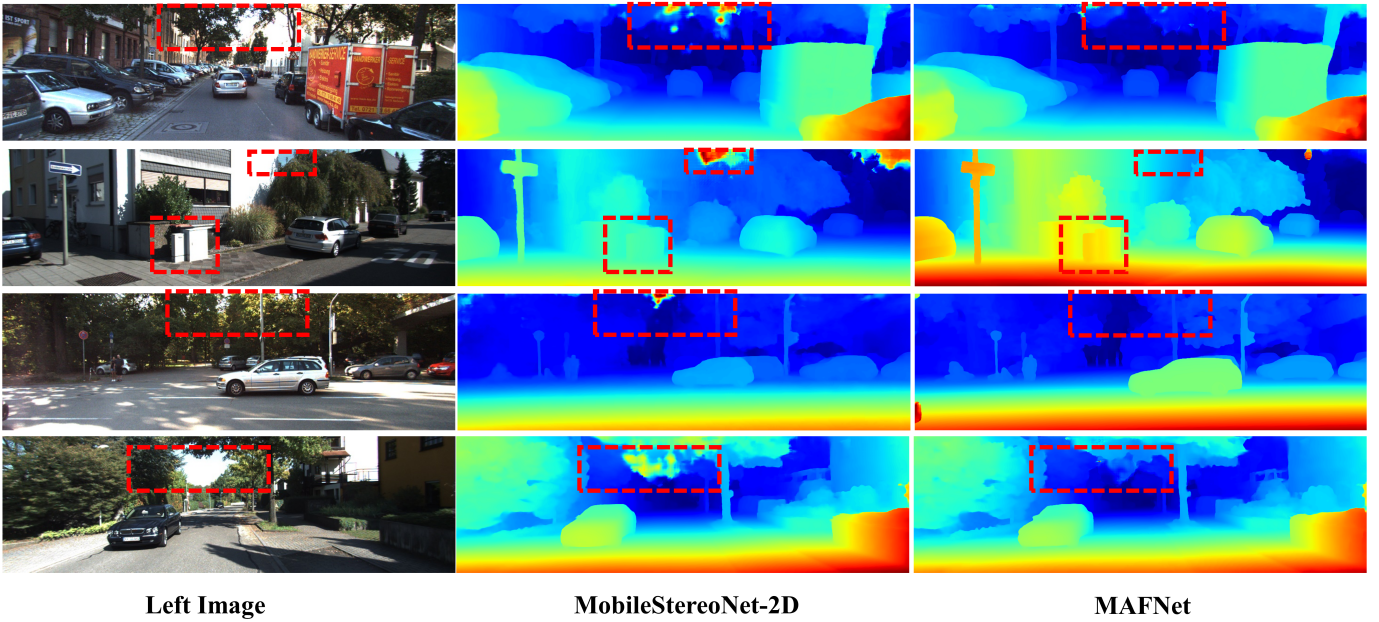


Fig. 5. Qualitative evaluation results on the KITTI 2012 [23] and KITTI 2015 [12] benchmarks. Through the introduction of a high- and low-frequency separation mechanism, MAFNet produces well-defined edges while maintaining complex structural details, enabling reliable matching even in extensive textureless regions and under drastic lighting changes.

Table II reports the results on the KITTI 2012 [23] and KITTI 2015 [12] datasets. These datasets reflect real driving scenes. The performance gains are larger than those on Scene Flow [11]. On KITTI 2015 [12], the D1-fg metric evaluates errors in foreground regions. These regions contain more object boundaries and fine details. The D1-fg value drops from 3.75% to 3.02%. This result corresponds to a 19% improvement. The improvement shows that the proposed method handles high-frequency details and object edges more effectively in foreground areas.

C. Comparisons with State-of-the-Art Methods

Quantitative Comparisons. Table III presents quantitative comparisons on the KITTI 2012 [23] and KITTI 2015 [12] benchmarks. MAFNet achieves the best overall performance among real-time and mobile-oriented stereo methods, while maintaining efficient inference speed. In particular, on KITTI 2015 [12], MAFNet obtains the lowest D1-all error of 1.81% with only 19 ms runtime, surpassing MobileStereoNet-2D [22] by 36.0% and BANet-2D [27] by 1.1%. These results demonstrate that MAFNet achieves a superior accuracy–efficiency trade-off and is well suited for real-time deployment on mobile and edge platforms. As illustrated in Fig. 1, the comparison results on Scene Flow demonstrate the effectiveness of the

proposed approach.

Qualitative Comparisons. The visual performance of the proposed MAFNet is compared with that of the mobile-oriented MobileStereoNet-2D [22]. As illustrated in Fig. 5, owing to its single feature aggregation mechanism, MobileStereoNet-2D tends to produce edge blurring and structural detail loss in high-frequency edges, thin structures, and large textureless areas. By contrast, thanks to the explicit decoupling and adaptive fusion of high- and low-frequency components, MAFNet can more precisely capture object boundaries while retaining intricate structural details. It exhibits more stable and coherent disparity estimation in high-frequency regions such as tree branches and traffic signs, as well as in scenes with significant illumination variations, resulting in more reliable matching performance.

IV. CONCLUSION

In this work, we introduced MAFNet, a novel stereo matching network that effectively balances accuracy and efficiency for real-time applications on resource-constrained devices. By leveraging an adaptive frequency-domain filtering attention module and a Linformer-based low-rank fusion mechanism, MAFNet can separately process high- and low-frequency information and integrate them for robust disparity estimation, while avoiding the computational burden of 3D convolutions. Extensive experiments on Scene Flow and KITTI 2015 benchmarks validate that MAFNet consistently outperforms existing real-time stereo matching methods, achieving superior accuracy with reduced computational cost. This demonstrates the potential of adaptive frequency-domain filtering attention and adaptive aggregation of high- and low-frequency in designing lightweight yet high-performance stereo networks, providing a promising solution for real-world mobile and embedded vision applications.

REFERENCES

- [1] Yunhua Lu, Xianzhong He, Qingwei Zhang, and Ding Zhang, "Fast stereo conformer: Real-time stereo matching with enhanced feature fusion for autonomous driving," *Engineering Applications of Artificial Intelligence*, vol. 149, pp. 110565, 2025.
- [2] Xiaoyi Zhang, Xuefeng Cao, Anzhu Yu, Wenshuai Yu, Zhenqi Li, and Yujun Quan, "Uavstereo: A multiple resolution dataset for stereo matching in uav scenarios," *IEEE Journal of Selected Topics in Applied Earth Observations and Remote Sensing*, vol. 16, pp. 2942–2953, 2023.
- [3] Hui Zhang, Li Zhu Liu, He Xie, Yiming Jiang, Jian Zhou, and Yaonan Wang, "Deep learning-based robot vision: High-end tools for smart manufacturing," *IEEE Instrumentation & Measurement Magazine*, vol. 25, no. 2, pp. 27–35, 2022.
- [4] Ziang Cheng, Jiayu Yang, and Hongdong Li, "Stereo matching in time: 100+ fps video stereo matching for extended reality," in *Proceedings of the IEEE/CVF Winter Conference on Applications of Computer Vision*, 2024, pp. 8719–8728.
- [5] Wenyao Xia, Elvis CS Chen, Stephen Pautler, and Terry M Peters, "A robust edge-preserving stereo matching method for laparoscopic images," *IEEE Transactions on Medical Imaging*, vol. 41, no. 7, pp. 1651–1664, 2022.
- [6] Chuang-Wei Liu, Qijun Chen, and Rui Fan, "Playing to vision foundation model's strengths in stereo matching," *IEEE Transactions on Intelligent Vehicles*, 2024.
- [7] Gangwei Xu, Xianqi Wang, Xiaohuan Ding, and Xin Yang, "Iterative geometry encoding volume for stereo matching," in *Proceedings of the IEEE/CVF conference on computer vision and pattern recognition*, 2023, pp. 21919–21928.
- [8] Tongfan Guan, Jiaxin Guo, Chen Wang, and Yun-Hui Liu, "Bridgedepth: Bridging monocular and stereo reasoning with latent alignment," in *Proceedings of the IEEE/CVF International Conference on Computer Vision*, 2025, pp. 27681–27691.
- [9] Bowen Wen, Matthew Trepte, Joseph Aribido, Jan Kautz, Orazio Gallo, and Stan Birchfield, "Foundationstereo: Zero-shot stereo matching," in *Proceedings of the Computer Vision and Pattern Recognition Conference*, 2025, pp. 5249–5260.
- [10] Junda Cheng, Longliang Liu, Gangwei Xu, Xianqi Wang, Zhaoxing Zhang, Yong Deng, Jinliang Zang, Yurui Chen, Zhipeng Cai, and Xin Yang, "Monster: Marry monodepth to stereo unleashes power," in *Proceedings of the Computer Vision and Pattern Recognition Conference*, 2025, pp. 6273–6282.
- [11] Nikolaus Mayer, Eddy Ilg, Philip Hausser, Philipp Fischer, Daniel Cremers, Alexey Dosovitskiy, and Thomas Brox, "A large dataset to train convolutional networks for disparity, optical flow, and scene flow estimation," in *Proceedings of the IEEE conference on computer vision and pattern recognition*, 2016, pp. 4040–4048.
- [12] Moritz Menze and Andreas Geiger, "Object scene flow for autonomous vehicles," in *Proceedings of the IEEE conference on computer vision and pattern recognition*, 2015, pp. 3061–3070.
- [13] Jiayi Zeng, Chengtang Yao, Lidong Yu, Yuwei Wu, and Yunde Jia, "Parameterized cost volume for stereo matching," in *Proceedings of the IEEE/CVF International Conference on Computer Vision*, 2023, pp. 18347–18357.
- [14] Gangwei Xu, Xianqi Wang, Zhaoxing Zhang, Junda Cheng, Chunyuan Liao, and Xin Yang, "Igev++: Iterative multi-range geometry encoding volumes for stereo matching," *IEEE Transactions on Pattern Analysis and Machine Intelligence*, 2025.
- [15] Xiaoyang Guo, Kai Yang, Wukui Yang, Xiaogang Wang, and Hongsheng Li, "Group-wise correlation stereo network," in *Proceedings of the IEEE/CVF conference on computer vision and pattern recognition*, 2019, pp. 3273–3282.
- [16] Gangwei Xu, Junda Cheng, Peng Guo, and Xin Yang, "Attention concatenation volume for accurate and efficient stereo matching," in *Proceedings of the IEEE/CVF conference on computer vision and pattern recognition*, 2022, pp. 12981–12990.
- [17] Zhelun Shen, Yuchao Dai, Xibin Song, Zhibo Rao, Dingfu Zhou, and Liangjun Zhang, "Pcw-net: Pyramid combination and warping cost volume for stereo matching," in *European conference on computer vision*. Springer, 2022, pp. 280–297.
- [18] Sameh Khamis, Sean Fanello, Christoph Rhemann, Adarsh Kowdle, Julien Valentin, and Shahram Izadi, "Stereonet: Guided hierarchical refinement for real-time edge-aware depth prediction," in *Proceedings of the European conference on computer vision (ECCV)*, 2018, pp. 573–590.
- [19] Shivam Duggal, Shenlong Wang, Wei-Chiu Ma, Rui Hu, and Raquel Urtasun, "Deeppruner: Learning efficient stereo matching via differentiable patchmatch," in *Proceedings of the IEEE/CVF international conference on computer vision*, 2019, pp. 4384–4393.
- [20] Gangwei Xu, Yun Wang, Junda Cheng, Jinhui Tang, and Xin Yang, "Accurate and efficient stereo matching via attention concatenation volume," *IEEE Transactions on Pattern Analysis and Machine Intelligence*, vol. 46, no. 4, pp. 2461–2474, 2023.
- [21] Haofei Xu and Juyong Zhang, "Aanet: Adaptive aggregation network for efficient stereo matching," in *Proceedings of the IEEE/CVF conference on computer vision and pattern recognition*, 2020, pp. 1959–1968.
- [22] Faranak Shamsafar, Samuel Woerz, Rafia Rahim, and Andreas Zell, "Mobilestereonet: Towards lightweight deep networks for stereo matching," in *Proceedings of the IEEE/CVF winter conference on applications of computer vision*, 2022, pp. 2417–2426.
- [23] Andreas Geiger, Philip Lenz, and Raquel Urtasun, "Are we ready for autonomous driving? the kitti vision benchmark suite," in *2012 IEEE conference on computer vision and pattern recognition*. IEEE, 2012, pp. 3354–3361.
- [24] Antyanta Bangunharcana, Jae Won Cho, Seokju Lee, In So Kweon, Kyung-Soo Kim, and Soohyun Kim, "Correlate-and-excite: Real-time stereo matching via guided cost volume excitation," in *2021 IEEE/RSJ International Conference on Intelligent Robots and Systems (IROS)*. IEEE, 2021, pp. 3542–3548.
- [25] Vladimir Tankovich, Christian Hane, Yinda Zhang, Adarsh Kowdle, Sean Fanello, and Sofien Bouaziz, "Hitnet: Hierarchical iterative tile refinement network for real-time stereo matching," in *Proceedings of*

the IEEE/CVF conference on computer vision and pattern recognition, 2021, pp. 14362–14372.

- [26] Bin Xu, Yuhua Xu, Xiaoli Yang, Wei Jia, and Yulan Guo, “Bilateral grid learning for stereo matching networks,” in *Proceedings of the IEEE/CVF conference on computer vision and pattern recognition*, 2021, pp. 12497–12506.
- [27] Gangwei Xu, Jiabin Liu, Xianqi Wang, Junda Cheng, Yong Deng, Jinliang Zang, Yurui Chen, and Xin Yang, “Banet: Bilateral aggregation network for mobile stereo matching,” *arXiv preprint arXiv:2503.03259*, 2025.
- [28] Ilya Loshchilov and Frank Hutter, “Decoupled weight decay regularization,” *arXiv preprint arXiv:1711.05101*, 2017.